

COVER PAGE

Document downloaded by @DAEL

Fri Nov 27 19:49:15 2026
For personal use

When automatic English translation is provided, only the original document is authentic.
The EAA cannot be held responsible of any translation error

Bibliographical reference

Joint Patch Near-Field Holography, Chao Yang, Jin Chen and Wen-Qiang Jia, Acta Acustica **vol. 95** (Number 2), 2009, pp. 234-240

DOI
https://doi.org/10.3813/AAA.918145

ACTA ACUSTICA UNITED WITH ACUSTICA
Vol. 95 (2009) 234 – 240

DOI 10.3813/AAA.918145

Joint Patch Near-Field Holography

Chao Yang, Jin Chen, Wen-qiang Jia
State Key Laboratory of Mechanical System and Vibration, Shanghai Jiao Tong University, Shanghai 200240, China

Summary
Traditional wave superposition method can't reconstruct the sound field precisely because of the absence of the equivalent source configuration information. A method named Joint Patch Near-field Holography (JPNAH) is proposed based on the statistically optimal near-field acoustical holography and the wave superposition method. The basic idea is that the fictitious sources' location essential to the wave superposition method can be decided by the statistically optimal near-field acoustical holography, and then complex sound field will be reconstructed by the wave superposition method with high efficiency and precision. Besides the reconstruction of the patch sound field, the JPNAH has many other virtues. Firstly, the JPNAH technique is not sensitive to the sound source outside the patch area. Secondly, compared to the NAH, the JPNAH performs better in the low frequency range. Finally, it is possible to achieve a real-time mapping of the complex sound field by using the JPNAH. Numerical simulations were performed based on a single-pulse-ball model; and also motor experiments were carried out in a semi-anechoic chamber. Both of numerical simulations and experiments show that the JPNAH can be used to reconstruct the sound field radiated from a complex sound source.

PACS no. 43.20.Rz, 43.40.Rj, 43.50.Yw

1. Introduction

Near-field acoustic holography (NAH) [1, 2, 3, 4], combined with a two-dimensional Fast Fourier Transformation (FFT) algorithm, was an early approach to the reconstruction of an acoustic field radiated from the surface of a planer source. A high-resolution image and accurate information of the sound source can be obtained by using NAH. Owing to the superiority in calculation, the Fast Fourier Transform-based NAH (FFT-based NAH) is the most popular method for the reconstruction of sound fields, and has been introduced into some software systems for industrial application. As described in NAH theory, the measurement must be implemented over an infinite area. But, this requirement cannot be met in reality; the use of the FFT-based NAH introduces some errors. The reason is that the discrete representation in the spatial frequency domain introduces periodic replica in the spatial domain, thus causing "wrap-around errors" in the calculation planes. In order to obtain accurate reconstruction results, the measurement must be made over a very large holographic plane. It is there obvious that the application of NAH to large vibrating structures is very difficult. Furthermore, NAH is unsuitable for reconstructing the acoustic properties of an arbitrary shape source. The statistically optimal near-field acoustical holography (SONAH) and wave superposition method (WSM) have been applied to overcome these obstacles [5].

Received 11 September 2008,
accepted 7 January 2009.

SONAH is good at locating the sound source at low and middle frequency by using the measurement array in small size. WSM proposed by Koopmann [6] is one kind of equivalent sources method. It is superior in accuracy and efficiency than any other boundary integral equation method because it does not require integration over singular integrands, and the method is easy to implement. However, the traditional wave superposition method can not reconstruct the sound field precisely because of the absence of equivalent source configuration information. Valdivia [7, 8] proposed two approximate methods that enabled one to carry out patch reconstruction for an arbitrary surface. The first approach is called patch IBEM with continuation procedure and the second is known as patch IBEM with direct procedure. Sarkissian [9, 10] applied the wave superposition method to reconstruct the field on a partial surface on a radiating structure from the measurement made on a limited surface.

A hybrid acoustic holography technique based on beamforming and the wave superposition method presented by Li [11] overcome the disadvantages of WSM and can be used to reconstruct the arbitrary sound source at the middle and high frequency. For the sound source at low and middle frequency, this paper presents a method named Joint Patch Near-field Holography (JPNAH) based on the statistically optimal near-field acoustical holography and the wave superposition method. The basic idea is that the fictitious sources' location essential to the wave superposition method can be decided by the statistically optimal near-field acoustical holography, and then the sound source at low and middle frequency will be reconstructed by the

© S. Hirzel Verlag · EAA

wave superposition method with high efficiency and precision.

2. Theory of the joint patch near-field holography

The SONAH and WSM will be introduced in this section. As mentioned in SONAH [12, 13, 14], the sound field can be written as a linear combination of plane propagating and plane evanescent wave, namely,

$$p(\boldsymbol{r}) = \frac{1}{4\pi^2}\int_{-\infty}^{+\infty}\int_{-\infty}^{+\infty} P(\boldsymbol{K})\,\Phi_K(\boldsymbol{r})\,\mathrm{d}\boldsymbol{K}, \tag{1}$$

where $p(\boldsymbol{r}) = p(x, y, z)$ is the sound pressure (Pa), $\boldsymbol{K} = (k_x, k_y)$ is a wave number vector, $k = \omega/c = 2\pi/\lambda$ is the wave number (rad/m), $\omega = 2\pi f$ is the angular frequency (rad/s), f is the frequency (Hz), c is the propagation speed of sound (m/s), λ is the wavelength (m), $P(\boldsymbol{K})$ is the plane wave spectrum, and

$$\Phi_K(x, y, z) = \mathrm{e}^{-\mathrm{i}(k_x x + k_y y + k_z z)} \tag{2}$$

are plane propagating and plane evanescent wave functions.

The k_z of the 3D wave number vector is given by

$$k_z = \begin{cases} \sqrt{k^2 - (k_x^2 + k_y^2)} & \text{for } \sqrt{(k_x^2 + k_y^2)} \le k, \\ -\mathrm{i}\sqrt{k_x^2 + k_y^2 - k^2} & \text{for } \sqrt{(k_x^2 + k_y^2)} > k. \end{cases} \tag{3}$$

The evanescent wave functions decay exponentially away from the source. The elementary wave functions Φ_K have amplitude of unity in the source plane. The plane wave spectrum $P(\boldsymbol{K})$ is a representation of the sound field in the spatial frequency domain.

The complex sound pressure $p(\boldsymbol{r}_n)$ obtained at N positions $\boldsymbol{r}_n = (x_n, y_n, z_n)$ on the measurement plane [5, 6, 7]. The pressure $p(\boldsymbol{r})$ at an arbitrary position $\boldsymbol{r} = (x, y, z)$ is estimated as a finite sum of the measured sound pressure data $p(\boldsymbol{r}_n)$,

$$p(\boldsymbol{r}) \approx \sum_{n=1}^{N} c_n(\boldsymbol{r})\, p(\boldsymbol{r}_n). \tag{4}$$

An infinite set of these elementary wave functions is used to provide good estimation for the formula (4),

$$\Phi_{K_m}(\boldsymbol{r}) \approx \sum_{n=1}^{N} c_n(\boldsymbol{r})\,\Phi_{K_m}(\boldsymbol{r}_n), \quad (m = 1, 2, \ldots, M,\ M \to \infty). \tag{5}$$

Solution to these equations in the "least squares" sense, for the coefficients $c_n(\boldsymbol{r})$ means that the estimation (4) is optimal for sound fields containing only the chosen function sub-set, and with approximately equal content of each function. Since all functions have amplitude equal to one on the source plane, the estimator is optimized for plane wave spectra.

Equation (5) can be arranged in matrix form,

$$\boldsymbol{b} = \begin{bmatrix} \Phi_{K_1}(\boldsymbol{r}) \\ \vdots \\ \Phi_{K_m}(\boldsymbol{r}) \end{bmatrix}, \tag{6}$$

$$\boldsymbol{c}(\boldsymbol{r}) = \begin{bmatrix} c_1(\boldsymbol{r}) \\ \vdots \\ c_N(\boldsymbol{r}) \end{bmatrix}, \tag{7}$$

$$\boldsymbol{A} = \begin{bmatrix} \Phi_{K_1}(\boldsymbol{r}_{h1}) & \cdots & \Phi_{K_1}(\boldsymbol{r}_{hN}) \\ \vdots & \vdots & \vdots \\ \Phi_{K_M}(\boldsymbol{r}_{h1}) & \cdots & \Phi_{K_M}(\boldsymbol{r}_{hN}) \end{bmatrix}, \tag{8}$$

Hence, equation (5) can be written as

$$\boldsymbol{b} = \boldsymbol{A}\,\boldsymbol{c}(\boldsymbol{r}). \tag{9}$$

The regularization solution to equation (9) is

$$\boldsymbol{c}(\boldsymbol{r}) = \left(\boldsymbol{A}^*\boldsymbol{A} + \alpha^2\boldsymbol{I}\right)^{-1}\boldsymbol{A}^*\boldsymbol{b}, \tag{10}$$

where $\boldsymbol{A}^*$ is the conjugate transpose of $\boldsymbol{A}$, $\boldsymbol{I}$ is the unit diagonal matrix and α is the regularization parameter which is given by [4]

$$\alpha^2 = \left(1 + \frac{1}{2(kd)^2}\right)10^{-\mathrm{SNR}/10}, \tag{11}$$

where SNR is the signal-to-noise-ratio in decibels for microphone signals, d is the distance between sound source plane and measurement plane.

The vector $c_n(\boldsymbol{r})$ of the prediction coefficients is solved; the pressure at the position $\boldsymbol{r}$ can be estimated through use of equation (4),

$$\begin{aligned} p(\boldsymbol{r}) &\approx \sum_{n=1}^{N} c_n(\boldsymbol{r})\, p(\boldsymbol{r}_n) = \boldsymbol{p}^T\boldsymbol{c}(\boldsymbol{r}) \\ &= \boldsymbol{p}^T\left(\boldsymbol{A}^*\boldsymbol{A} + \alpha^2\boldsymbol{I}\right)^{-1}\boldsymbol{A}^*\boldsymbol{b}. \end{aligned} \tag{12}$$

Here, $\boldsymbol{p}^T = [p(\boldsymbol{r}_1) \ldots p(\boldsymbol{r})]$ is a vector containing the measured pressure signals.

The basic idea of WSM [6] is that the sound field radiated from an arbitrary object can be expressed as a linear superposition of some sound fields produced by a source distribution placed on a surface inside the object. The fictitious sources' strength and the coefficients associated with these independent sources are determined by requiring the assumed form of the solution to satisfy the pressure or velocity boundary condition at the measurement plane, and the errors incurred in this process are minimized by the least-squares method.

The field on the measurement plane can be expressed as

$$\boldsymbol{p} = \boldsymbol{H}\,\boldsymbol{q}, \tag{13}$$

$$\boldsymbol{V}_n = \boldsymbol{T}\,\boldsymbol{q}, \tag{14}$$

where $\boldsymbol{p}$ and $\boldsymbol{V}_n$ are the vector of the measured sound pressure and the measured particle velocity, $\boldsymbol{H}$ and $\boldsymbol{T}$ are the

transfer function matrix, $\boldsymbol{q}$ is vector of the fictitious source strength.

The fictitious source strengths are determined by applying boundary condition on the measurement plane. We invert matrix $\boldsymbol{H}$ or $\boldsymbol{T}$, and rewrite equation (13) and equation (14) as

$$\boldsymbol{q} = \boldsymbol{H}^{-1}\,\boldsymbol{p} = \boldsymbol{T}^{-1}\,\boldsymbol{p}. \tag{15}$$

Once the fictitious source strengths are determined using equation (15), the sound pressure near the source can be approximated by

$$\boldsymbol{p}^{R} = \boldsymbol{H}^{R}\,\boldsymbol{q}. \tag{16}$$

The reconstruction precision of WSM is determined by the original location of the fictitious source. How to configure the fictitious source is an unsettled problem in the traditional WSM. The basic idea of the Joint Patch Near-field Holography (JPNAH) is that the fictitious sources' location can be decided by the statistically optimal near-field acoustical holography and then the sound source can be reconstructed with high efficiency and precision. There are two hypotheses on JPNAH: 1) the number of the discrete sound source of the object is finite; 2) the radiated frequency ranges from low to middle frequency band.

The Principle diagram of JPNAH is shown in Figure 1. S_1 and S_2 represent the arbitrary shaped sound source. The location of the two sound sources can be obtained by using SONAH with the data measured on holography plane a, and its x-axis projection on the holography plane a are represented by X_{a1} and X_{a2}. Then, the holography plane b will be obtained by rotating the holography plane a along the y-axis. The angle between the two holography planes is α. In the same vein, we can obtain Xb1, Xb2. The three-dimensional coordinates of the two sound sources can be calculated by using equations (17)–(21) based on X_{a1}, X_{a2}, X_{b1}, X_{b2} and α.

Equations (17)–(21) are given as

$$X_{ab} = \sqrt{X_a(j)^2 + X_b(j)^2 - 2\cos(180-\alpha)X_a(j)X_b(j)}, \tag{17}$$

$$\beta = 90 - \arccos\frac{X_{ab}^2 + X_a(j)^2 - X_b(j)^2}{2X_a(j)X_{ab}}, \tag{18}$$

$$\gamma = 180 - \alpha - \beta, \tag{19}$$

$$D_a(j) = \frac{\sin\beta}{\sin\gamma} D_b(j), \tag{20}$$

$$D_a(j) = \sqrt{\frac{X_a(j)^2 + X_b(j)^2 - 2\cos(180-\alpha)X_a(j)X_b(j)}{1 + (\sin\beta/\sin\gamma)^2 - 2\cos\alpha\ \sin\beta/\sin\gamma}}, \tag{21}$$

where j represents the sound source number.

In particular, if the distance between the source and holography plane can be easily measured, the x-axis and y-axis coordinates of the sound sources can be obtained by projecting the sources to the holography plane.

Flow chart of the implementation of the JPNAH is shown in Figure 2, and the procedure is briefly explained below. 1) design of the measurement array; 2) measurement of the sound pressure; 3) the Fast Fourier Transform of the data; 4) selection of the analyzed frequency; 5) obtain the X_{a1}, X_{a2}, X_{b1}, X_{b2} and α; 6) calculate the three-dimensional coordinates of the sources; 7) configure the fictitious source and reconstruct the sound field by WSM.

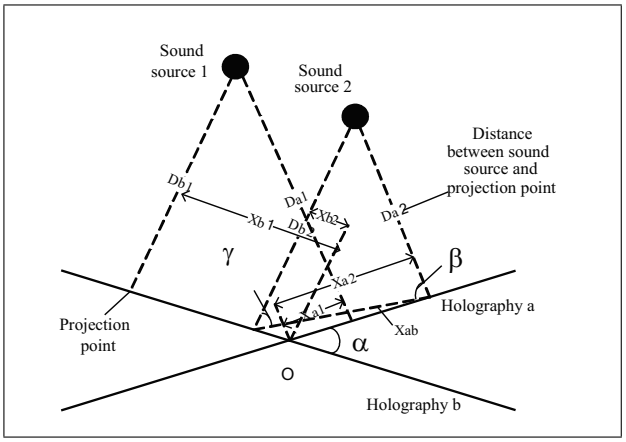

Figure 1. Principle diagram of sound source localization based on JPNAH.

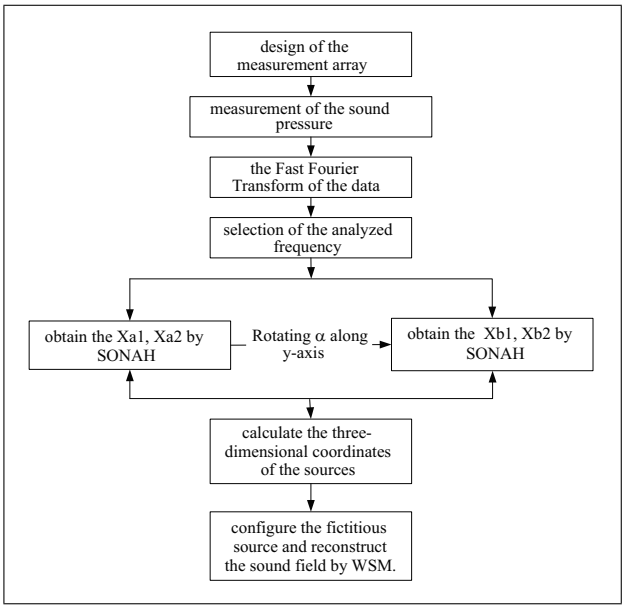

Figure 2. Flow chart of the implementation of the JPNAH.

3. Numerical simulations

3.1. Simulation setup

For simulations, a pulse sound source has been built up. The radius is 0.04 m and the pulse velocity is 0.025 m/s. The frequency ranges from 200 to 1000 Hz, and the grid is designed as a 5×5 elements array with 0.1 m grid spacing, the source is located at (0, 0, 0). The array is positioned 0.3 m in front of the source. JPNAH, SONAH and the traditional WSM calculations are performed in the reconstruction plane $z = 0.05$ m.

The relative average error level is calculated from the formula

$$e = 10\log_{10}\left(\frac{\sum\left|p_i^{ture} - p_i\right|^2}{\sum\left|p_i^{ture}\right|^2}\right), \qquad (22)$$

where e is the relative error, p_i^{ture} is the theoretical sound pressure, p_i is the reconstructed sound pressure.

3.2. Comparisons of the JPNAN, SONAH and WSM

Based on the data obtained on the holography plane a, the projection of the source is at (0, 0) on the holography plane a, and based on the data obtained on the holography plane b, the projection of the source is at (-0.15, 0) on the holography plane b. The angle between the two holography planes is 30 degrees. With equations (17)–(21), the three-dimensional coordinates of the sources are (0, 0, 0.3) (based on holography plane a) or (-0.15, 0, 0.26) (based on holography plane b). The first three-dimensional coordinates (0, 0, 0.3) is used in the next step.

Figure 3 shows the 3-D plots of the reconstruction and the relative average error level by JPNAH, SONAH and the traditional WSM. Figure 3a shows the reconstruction of the traditional WSM at 1000Hz. Figure 3b shows the reconstruction of the SONAH at 1000 Hz. Figure 3c shows the reconstruction of the JPNAH at 1000 Hz. The relative average error levels of the WSM, SONAH and the JPNAH are compared in Figure 3d. The dashed circle line, dashed star line and solid star line represent SONAH, the traditional WSM and the JPNAH, respectively.

As shown in Figure 3a, the reconstructed sound pressure is larger than the theoretical one. The traditional WSM can not reconstruct the sound field because of the absence of the location information of the source. Figure 3b shows that the reconstruction by SONAH is not good. The reason is that the sound field is not radiated by a planar object. On the contrary, the JPNAH can reconstruct the sound field well (shown in Figure 3c). The reconstructed and theoretical sound pressure is almost same. Figure 3d shows that the relative average error levels of JPNAH, SONAH and the traditional WSM are less than -120 dB and -20 dB over the frequency ranges from 200 Hz to 1000 Hz, respectively. So, the JPNAH is better than the traditional WSM and SONAH on reconstruction precision at the low-middle frequency band. Furthermore, the errors of the JPNAH over the frequency band are stable.

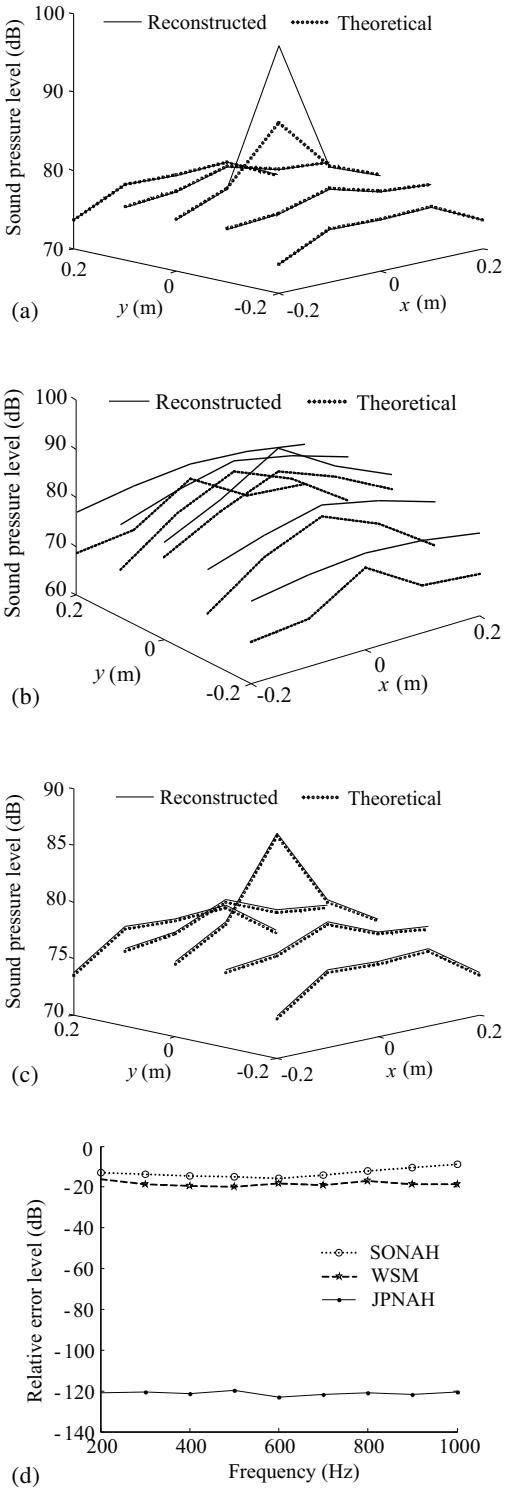

Figure 3. Comparisons of the WSM, SONAH and JPNAH. a) Reconstruction result of the WSM at 1000 Hz, b) Reconstruction result of the SONAH at 1000 Hz, c) Reconstruction result of the JPNAH at 1000 Hz, d) Reconstruction error of the three methods over the frequency ranges from 200 to 1000 Hz.

3.3. The effect of data missing on the JPNAH

The JPNAH is applied here which may be used to either extrapolate the sound field to enlarge the measurement surface or to interpolate in case there is a "hole" in the measurement surface where data are not available. The simulation setup is same to section 3.1. Figure 4 shows the reconstruction and the relative average error level by JPNAH based on the different data missing. Figures 4a,b show the setup of the different data missing. Figures 4c,d show the reconstruction result of the JPNAH at 1000 Hz, and the relative average error levels of the JPNAH are shown in Figures 4e,f.

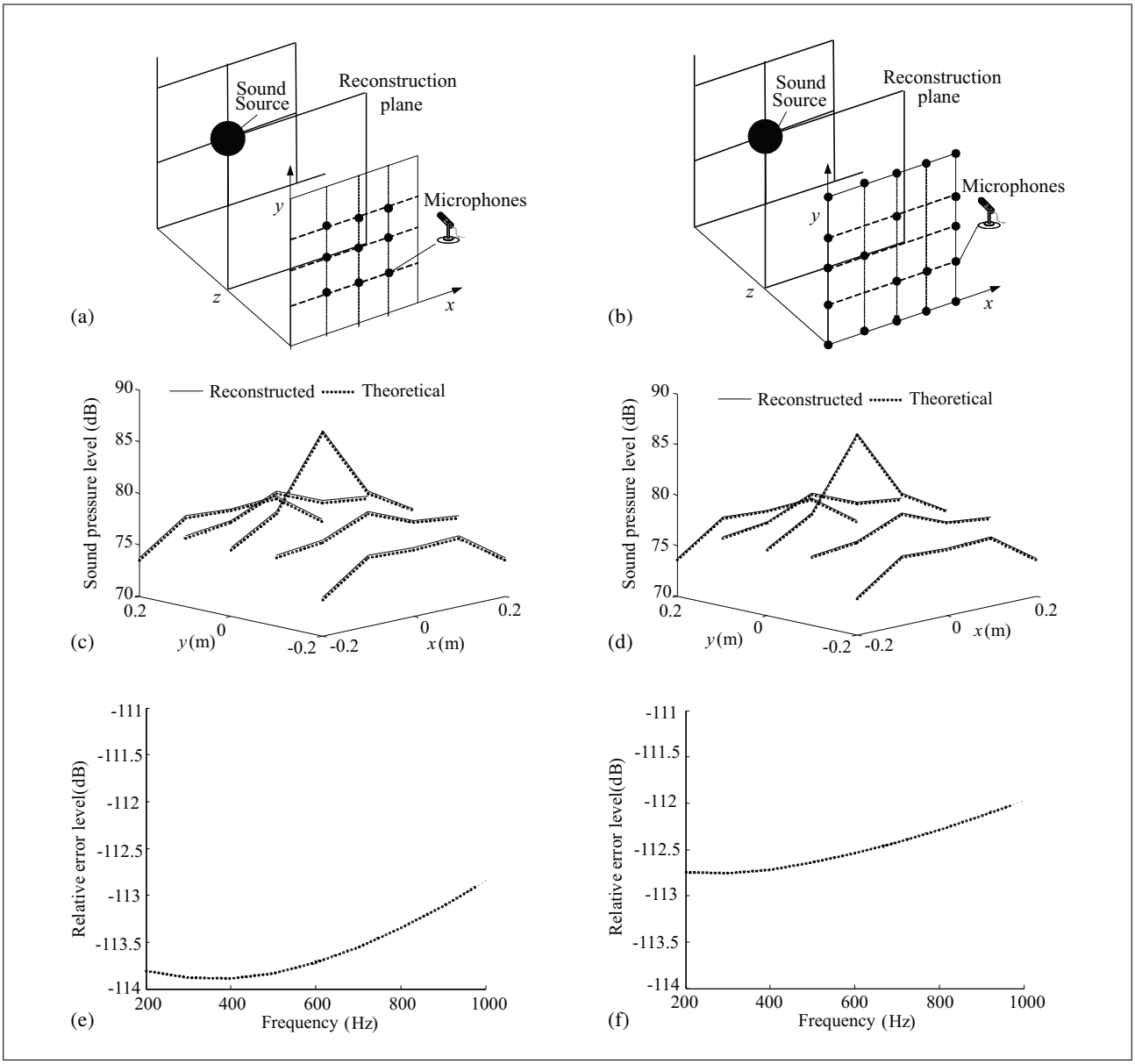

Figure 4. Reconstruction based on JPNAH when the some measurement data is missing. a) The measurement data on the peripheral section are not available. b) The measurement data on the central section are not available. c) Reconstruction result at 1000 Hz when the measurement data on the peripheral section are not available. d) Reconstruction result at 1000 Hz when the measurement data on the central section are not available. e) Reconstruction error over the frequency ranges from 200 to 1000 Hz when the measurement data on the peripheral section are not available. f) Reconstruction error over the frequency ranges from 200 to 1000 Hz when the measurement data on the central section are not available.

As shown in Figures 4c,d, the reconstruction by the JPNAH is very good. The theoretical and reconstructed sound pressure fit well. These prove that JPNAH can be used to either reconstruct a larger surface (the measurement data on the peripheral section of the measurement plane are not available) or reconstruct a smaller surface (the measurement data on the central section of the measurement plane are not available). The JPNAH is a good method for reconstruction of partial sound field. Figures 4e,f show that the relative average error levels of the JPNAH is less than -112 dB over the frequency ranges from 200 Hz to 1000 Hz when the data is missed on the peripheral or central section.

4. Experiments

4.1. Experiment setup

All experiments were performed in the semi-anechoic chamber of the State Key Laboratory of Mechanical System and Vibration at Shanghai Jiao Tong University. The array is designed as a 5×5 element microphone array with 0.2m grid spacing, the microphones being at the corners of the grid. As shown in Figure 5, the array is positioned 0.4 m in front of the motor. The dimension of the motor is 0.5 m×0.15 m×0.2 m and the center of the motor is the Coordinate Origin. JPNAH calculations were performed in the reconstruction plane $z = 0.35$ m. The reconstruc-

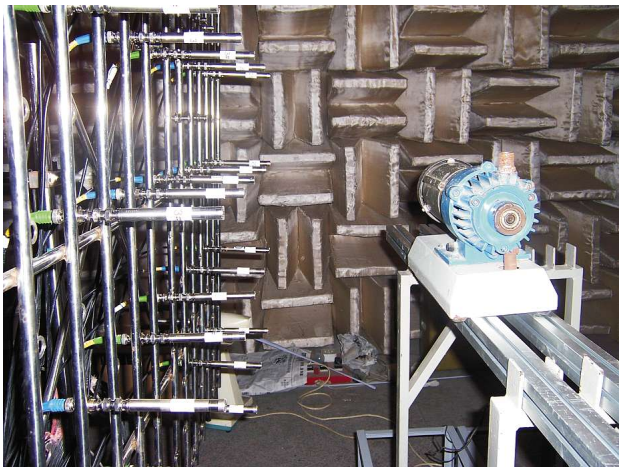

Figure 5. The motor and microphone array.

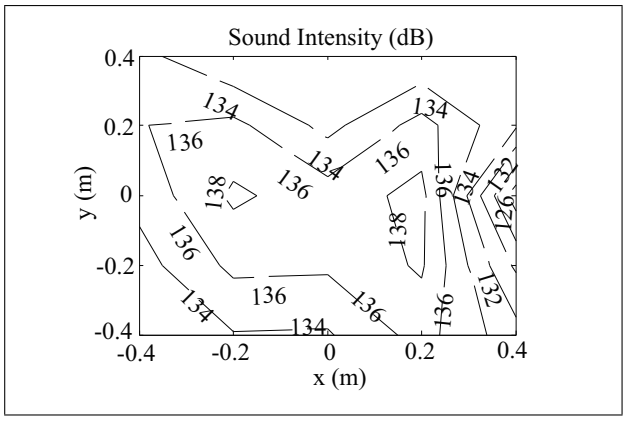

Figure 6. The sound sources of the motor at 736 Hz.

tion grid has the same geometry as the measurement grid. Free-field 1/2" Microphone Type MP201 used in the experiment is a pre-polarized microphone for general sound measurements and for standardized noise measurements. With its low inherent noise and frequency range from 20 to 20000 Hz, it is very well suited for a wide range of precision audio-frequency sound measurements. Its nominal open-circuit sensitivity is 50 mV/Pa.

4.2. Experiment results

The location of the motor by using the JPNAH is shown in Figure 6. There are two sound sources, one is at (-0.2, 0, 0), the other is at (0.2, 0, 0). Next, the sound field will be reconstructed by the JPNAH. Figure 7 shows the reconstructed and measured sound pressure by different methods at 736 Hz.

The frequency of interest is 736 Hz. As shown in Figure 7a, there are two sound sources in this figure, which locate in front-end and back-end of the motor. Though the analysis the front-end sound source and the back-end sound source are generated by the bearing and the fan of the running motor. The reason is 1. the eccentricity of the front-end rotor; 2. the imbalance of the back-end fan. Figures 7b,c show that the reconstruction sound pressure level

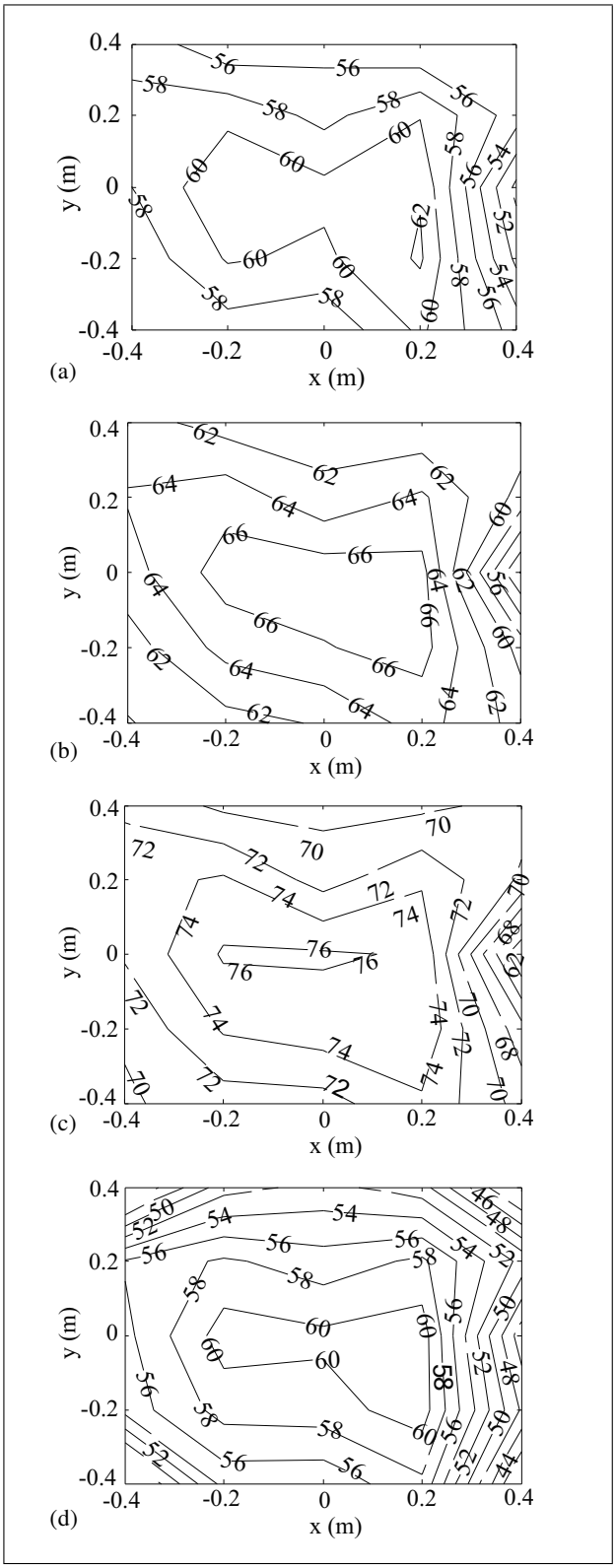

Figure 7. Reconstruction of the sound field by different methods. a) The contour of the measured sound pressure. b) The contour of the reconstructed sound pressure by WSM. c) The contour of the reconstructed sound pressure by SONAH. d) The contour of the reconstructed sound pressure by JPNAH.

based on the WSM or SONAH is larger than the measured one over the reconstruction plane. These two methods can-

not give the precise sound pressure radiated by the motor. Compared with Figure 7a, Figure 7d shows the same information about the motor. The experiments show that the JPNAH can be used to reconstruct the sound field radiated by an arbitrary shaped object. The diagnosis of machinery based on the JPNAH will become true by comparing the reconstructed images with the normal images.

5. Conclusions

The traditional wave superposition method cannot reconstruct the sound field precisely because of the absence of equivalent source configuration information. The SONAH cannot be used to reconstruct the sound field radiated by a complex sound source.

The JPNAH calculation method overcomes these limitations as it can operate with irregular array and allows for measurements with arrays smaller than the source, without severe spatial windowing effects. Besides the reconstruction of the patch sound field, the JPNAH method has many other virtues. Firstly, it is not sensitive to the sound source outside the patch area. Secondly, compared with NAH, the JPNAH performs better in low-middle frequency range. JPNAH can simplify measurements and decrease the cost of the experiments. Finally, it is possible to achieve a real-time mapping of the sound field radiated from an arbitrary shaped object by using JPNAH.

Acknowledgement

This work was supported by National Natural Science Foundation of China, Project NO.50675140 and the National High Technology Research and Development Program of China (Grant No. 2006AA04Z175).

References

[1] E. G. Williams: Sound source constructions using a microphone array. Journal of the Acoustical Society of America **68** (1980) 340–344.

[2] E. G. Williams, J. D. Maynard: Holographic imaging without the wavelength resolution limit. Physical Review Letter **45** (1980) 554–557.

[3] J. D. Maynard, E. G. Williams, Y. Lee: Near-field acoustic holography: Theory of generalized holography and the development of NAH. Journal of the Acoustical Society of America **78** (1985) 395–1413.

[4] J. Li, Jia-qing amd Chen, C. Yang et al.: Analysis of the impact factors on the accuracy of sound field reconstruction based on wave superposition. Acta Physica Sinica **57** (2008) 4258–4264.

[5] C. Yang, J. Chen, W. F. Xue et al.: Progress of the patch near-field acoustical holography technique. Acta Acustica United with Acustica **94** (2008) 156–163.

[6] G. H. Koopmann, L. Song, J. B. Fahnline: A method for computing acoustic fields based on the principle of wave superposition. Journal of the Acoustical Society of America **86** (1989) 2433–2438.

[7] N. P. Valdivia, E. G. Williams, P. C. Herdic: Approximations of inverse boundary element methods with partial measurements of the pressure field. Journal of the Acoustical Society of America **123** (2008) 109–120.

[8] N. P. Valdivia, E. G. Williams: Study of the comparison of the methods of equivalent sources and boundary element methods for near-field acoustic. Journal of the Acoustical Society of America **120** (2006) 3694–3705.

[9] A. Sarkissian: Extension of measurement surface in near-field acoustic holography. Journal of the Acoustical Society of America **115** (2004) 1593–1596.

[10] A. Sarkissian: Method of superposition applied to patch near-field acoustic holography. Journal of the Acoustical Society of America **118** (2005) 671–678.

[11] J.-q. Li, J. Chen, C. Yang et al.: A hybrid acoustic holography technique based on beam-forming and wave superposition algorithm. Acta Acustica **33** (2008) 152–158.

[12] R. Steiner, J. Hald: Near-field acoustical holography without the errors and its limitations caused by the use of spatial DFT. International Journal of Acoustics and Vibration **6** (2001) 83–89.

[13] C. Y. Thung, J. Hald: Source visualization by using statistically optimized near-field acoustical holography in cylindrical coordinates. Journal of the Acoustical Society of America **118** (2005) 2355–2364.

[14] W. B. Li, J. Chen, F. Yu: The principle of statistically optimal planar near-field acoustical holography and the sound field separation technique. Acta Physica Sinica **54** (2005) 1253–1260.